

Instability to a heterogeneous oscillatory state in randomly connected recurrent networks with delayed interactions

Célian Bimbard,¹ Erwan Ledoux,² and Srdjan Ostojic²

*¹Laboratoire des Systèmes Perceptifs,
Équipe Audition, CNRS UMR 8248,
École Normale Supérieure, Paris, France.*

*²Group for Neural Theory, Laboratoire de Neurosciences Cognitives,
INSERM U960, École Normale Supérieure, Paris, France.*

(Dated: November 5, 2021)

Abstract

Oscillatory dynamics are ubiquitous in biological networks. Possible sources of oscillations are well understood in low-dimensional systems, but have not been fully explored in high-dimensional networks. Here we study large networks consisting of randomly coupled rate units. We identify a novel type of bifurcation in which a continuous part of the eigenvalue spectrum of the linear stability matrix crosses the instability line at non-zero-frequency. This bifurcation occurs when the interactions are delayed and partially anti-symmetric, and leads to a heterogeneous oscillatory state in which oscillations are apparent in the activity of individual units, but not on the population-average level.

I. INTRODUCTION

Networks of interacting units are a fundamental model of many physical and biological systems, and understanding their dynamical repertoire is of outmost importance. Dynamical systems theory has examined extensively the dynamics of low-dimensional systems, and in particular bifurcations between different regimes [1]. These bifurcations typically occur when an eigenvalue of the system (or pair thereof) crosses an instability line, and enumerating the possible scenarios leads to an exhaustive taxonomy of dynamical behaviors for low-dimensional networks.

Many biological systems, in particular regulatory and neural networks, are however high-dimensional as they consist of a large number of individual units, and the interactions between units are moreover strongly disordered. In contrast to low-dimensional systems, the dynamical repertoire of high-dimensional networks of randomly interacting units has not been fully charted, and new phenomena have been recently discovered. In particular, within the context of randomly connected neural networks, a novel bifurcation has been identified, in which a continuum of eigenvalues loses stability, leading to a transition from constant, fixed-point activity to highly heterogeneous, chaotic activity [2]. This transition and its implications for neural computations have lately attracted a significant amount of attention [3–8].

In the bifurcation to chaotic activity described above, the continuous part of the spectrum that loses stability is centered around the real axis in the complex plane, and leads to an instability at zero-frequency. Here we show that an analogous, but non-zero frequency instability can occur when interactions are delayed and partially anti-symmetric. This novel type of bifurcation leads to a new type of heterogeneous oscillatory state, in which different units oscillate at similar frequencies but random phases.

II. NETWORK MODEL

We investigated the dynamics of a network of N randomly connected rate units [9] given by

$$\frac{dx_i(t)}{dt} = -x_i(t) + \sum_{j=1}^N J_{ij} \phi(x_j(t-D)) \quad i = 1 \dots N \quad (1)$$

where x_i is the activity of unit i , $\phi(x) = \tanh(x)$ is the transfer function, and D represents a delay in the interaction between the units. The elements of the interaction matrix J are drawn from a Gaussian distribution of mean 0 and variance g^2/N . The symmetric elements J_{ij} and J_{ji} are correlated, and the degree of symmetry $\tau_s = \langle J_{ij}J_{ji} \rangle N/g^2$ is a parameter that we systematically varied. For $\tau_s = 1$, the interaction matrix is fully symmetric, for $\tau_s = 0$ it is fully asymmetric, and for $\tau_s = -1$ it is fully anti-symmetric.

The network possesses a trivial fixed point for which the activity of all the units vanishes. We examined the stability of this fixed point as function of the strength of coupling g , the degree of symmetry in the interactions τ_s , and the delay D . We considered heterogeneous perturbations in which the activity of each unit is perturbed away from the fixed point by an amount $\delta x_i(t) = \delta \tilde{x}_i e^{\lambda t}$, with λ an arbitrary complex number representing the decay of the perturbation.

Inserting the perturbation in Eq. 1 and linearizing around the fixed point we get

$$e^{\lambda D} (1 + \lambda) \delta \tilde{x}_i = \sum_{j=1}^N J_{ij} \delta \tilde{x}_j. \quad (2)$$

Diagonalizing the interaction matrix J , and projecting on the k -th eigenmode yields

$$e^{\lambda_k D} (1 + \lambda_k) = \mu_k \quad (3)$$

where μ_k is the k -th eigenvalue of J . We therefore obtain N independent characteristic equations that specify N admissible values of the perturbation decay λ_k , $k = 1 \dots N$, one for each eigenvalue of J . For a given set of parameters g, τ_s and D , if any of these equations admits a solution with $\Re \lambda_k > 0$, the corresponding perturbation is amplified and the fixed point is unstable.

In the limit of large N , the eigenvalues μ_k of the matrix J are uniformly distributed within an ellipse centered at the origin in the complex plane, with real and imaginary axes $g(1 + \tau_s)$ and $g(1 - \tau_s)$ respectively [10]. Solving Eq. 3 for λ yields a mapping that transforms this ellipse into a different domain in the complex plane, that contains the solutions λ_k of Eq. 3 (Fig. 1). We will call μ -domain the domain containing the eigenvalues μ_k of J , and

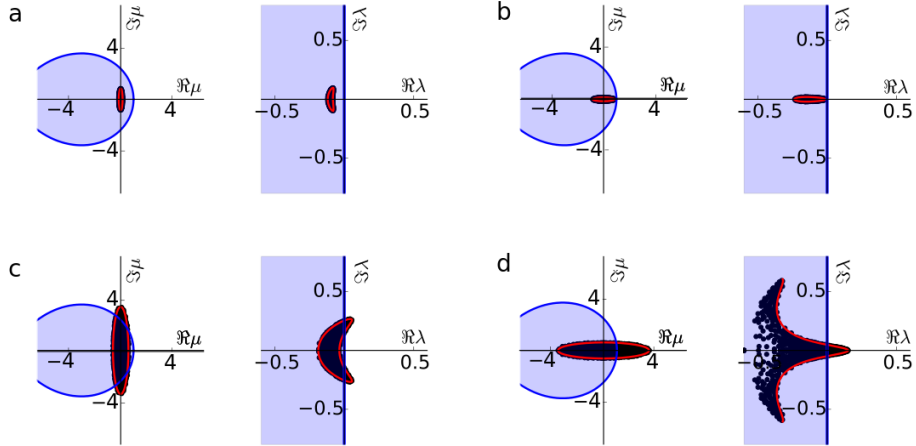


FIG. 1. Linear stability of the fixed point solution. a-d. Left panel: Eigenvalues μ of a simulated interaction matrix (black dots), theoretically-determined domain containing the eigenvalues (red ellipse) and stability domain (blue shaded region). Right panel: perturbation decay λ associated to each eigenvalue μ (black dots), theoretical prediction of the λ associated to the contour of the μ -ellipse (red line) and stability domain (blue shaded region). Parameter values a. $\tau_s = -0.7$ and $g = 0.2$ ($N = 1000$, $D = 0.2$) b. Same as in a., with $\tau_s = 0.7$ and $g = 0.2$ c. Same as in a., with $\tau_s = -0.7$ and $g = 2.0$ d. Same as in a., with $\tau_s = 0.7$ and $g = 2.0$.

λ -domain the domain containing the solutions λ_k of Eq. 3. Note that the μ -domain depends only on the values of g and τ_s , while the λ -domain depends also on the interaction delay D .

III. PHASE DIAGRAM

One approach for assessing the stability of the fixed point for a given set of parameters is to examine whether the resulting λ -domain intersects the line $\Re z = 0$ in the complex plane. An alternative approach is to use the inverse mapping and determine the contour $\mu(z)$ in the μ -plane that corresponds to $\Re \lambda = 0$, and examine whether this contour intersects the μ -domain containing the eigenvalues.

The two approaches are graphically illustrated in Fig. 1. For small values of the coupling g , the eigenvalues μ_k of J have a small modulus, and all λ_k solution of Eq. 3 have a negative real part: the synaptic coupling is too low to drive any instability of the fixed point. When the coupling g is increased, the λ domain crosses the imaginary axis (fig. 1-c,d). In this case, the degree of symmetry of the matrix appears to play an important role for the shape

of the λ -domain: in the antisymmetric case (fig. 1-c), values with $\Re\lambda > 0$ have a non-zero imaginary part, whereas in the symmetric case (fig. 1-d), the solution λ_0 with largest real part has a vanishing imaginary part. We predict that these two cases are unstable, the antisymmetric case possibly leading to an oscillatory behavior.

To systematically identify bifurcation points, we determined the coupling strength g_c for which $\lambda = i\omega_c$ is a solution of a characteristic equation Eq. 3. We first consider two simplifying cases, before describing the general solution.

For a symmetrically skewed matrix ($0 < \tau_s < 1$), the ellipse that contains the eigenvalues of the matrix J is elongated along the real axis. The eigenvalue μ_0 with the largest modulus is therefore purely real, and given by $\mu_0 = g(1 + \tau_s)$. The corresponding solution λ_0 of Eq. 3 is also real, and vanishes when $\mu_0 = 1$, which yields the critical coupling $g_c = 1/(1 + \tau_s)$. At this coupling, all other solutions of Eq. 3 have negative real parts, hence we have a zero-frequency bifurcation.

For an anti-symmetrically skewed matrix ($-1 < \tau_s < 0$), the ellipse that contains the eigenvalues of the matrix J is elongated along the imaginary axis, and the eigenvalue μ_0 with the largest modulus is therefore purely imaginary and given by $\mu_0 = ig(1 - \tau_s)$. The corresponding solution λ_0 of Eq. 3 now has a non-zero imaginary part, and the solution $\lambda_0 = i\omega_c$ is given by

$$\omega_c = \sqrt{(g(1 - \tau_s))^2 - 1} \quad (4)$$

$$D = \frac{1}{\sqrt{(g(1 - \tau_s))^2 - 1}} \arcsin\left(\frac{1}{g(1 - \tau_s)}\right). \quad (5)$$

This solution leads to a bifurcation with a non-zero frequency.

More generally, the first eigenvalue that becomes unstable as the coupling g is increased does not need to correspond to an extremity of the ellipse in the μ -plane. To determine the location of the instability in the general case, we followed [11, 12], and determined the contour $\mu(z)$ in the complex plane that is mapped to the line $\lambda = i\omega$ via Eq. 3. Parametrizing this contour in polar coordinates as $\mu(\theta) = M(\theta)e^{i\theta}$, we have for $0 < \theta < \pi$ (the contour is symmetric to the horizontal axis)[12]

$$\begin{aligned}
M(\theta) &= \sqrt{1 + \omega^2} \\
-\omega &= \tan(\omega D - \theta), \quad \text{with } \theta - \frac{\pi}{2} < \omega D < \theta, \quad \text{modulo } 2\pi.
\end{aligned}
\tag{6}$$

This contour depends only on the value of the delay D , and defines a droplet-shaped stability boundary for the eigenvalues of J (Fig. 1). The critical coupling g_c is then determined by the first intersection as coupling is increased between the elliptical μ -domain containing the eigenvalues, and the stability boundary defined by Eq. 6.

The full bifurcation diagram as function of symmetry τ_s and coupling g for a fixed value of the delay D is displayed in Fig. 2. For the symmetric case, $\tau_s > 0$, the instability is given by the extremity of the ellipse on the real axis. It therefore occurs at zero frequency, and the critical coupling is given by $g_c = 1/(1 + \tau_s)$. For couplings larger than g_c , the fixed point is unstable, and a chaotic, fluctuating state appears [2].

The zero-frequency, chaotic instability extends to the anti-symmetric region until a critical value $\tau_s^c < 0$ for which a non-zero frequency bifurcation appears. As τ_s is further decreased, the non-zero frequency instability is determined by eigenvalues closer and closer to the extremity of the ellipse along the imaginary axes, so that the critical coupling and the frequency of the instability are well approximated by Eqs. 4-5.

The critical coupling g_c and the frequency ω_c of the bifurcation strongly depend on the value of the delay D in the interactions (Fig. 3). As the value of D is increased from 0, for a given value of τ_s both g_c and ω_c progressively decrease. At the same time, τ_s^c increases, so that the oscillatory instability occupies an increasing portion of phase space. In the limit of infinitely long delays, τ_s^c tends to zero, so that the oscillatory instability extends until the boundary between antisymmetric and symmetric interactions.

IV. HETEROGENEOUS OSCILLATORY STATE

In the region of the oscillatory instability, couplings larger than g_c lead to a novel type of heterogeneous oscillatory state that we investigated using numerical simulations of Eq. 1. In this state, the different units appear to oscillate with essentially identical frequencies, but random phases and amplitudes (Fig. 4). To further characterize this state, we defined the phase of each unit as the phase of the first peak (t_{peak}) with respect to an arbitrary reference

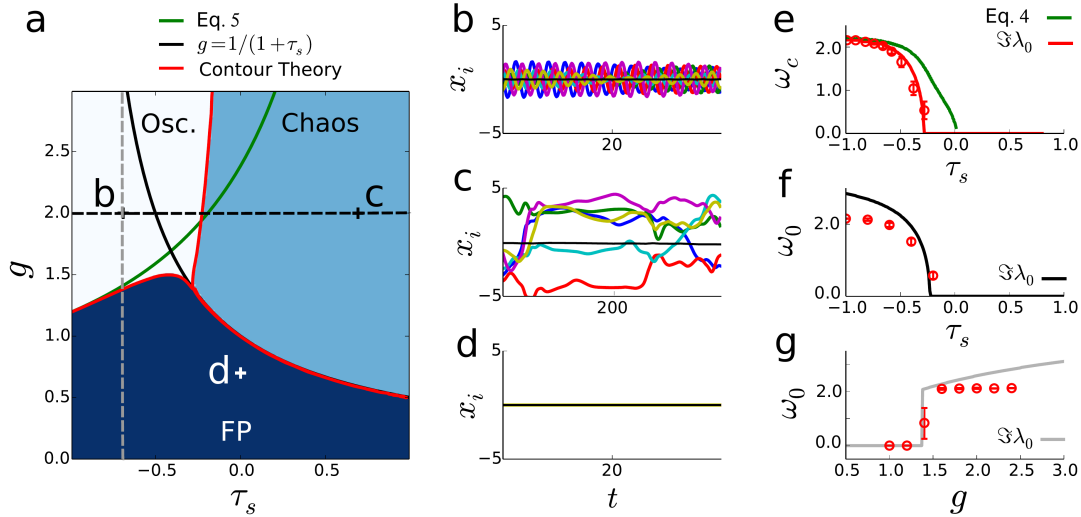


FIG. 2. Dynamical regimes of the network. a. Bifurcation Diagram. Dark blue region: fixed point (FP) is stable; light blue region: FP is unstable, with dominant eigenvalue real; white region: FP is unstable, dominant eigenvalue with a non-zero imaginary part. Red line: exact theoretical prediction for the instability line. Black line: approximation for $\tau_s > 0$, Green line: approximation for $\tau_s < 0$. b-d: Illustrations of simulated dynamics in different regions of the bifurcation diagram ($N = 1000$, $D = 0.2$). The panels show firing rates of ten neurons and the population average in black. Parameter values: b. $\tau_s = -0.7$ and $g = 2.0$, c. $\tau_s = 0.7$ and $g = 2.0$, d. $\tau_s = 0.7$ and $g = 0.7$. e. Bifurcation frequency ω_c computed along the instability line in panel a (red line), and approximation given by $\omega_0 = \sqrt{(g(1-\tau_s))^2 - 1}$ (green line). Simulation results are shown as red dots ($N = 500$, $n = 5$, mean \pm sem). f. Frequency of the dominant eigenvalue for constant g as function of τ_s (along the black dashed line in panel a), compared to the frequency of oscillations in the simulated network (red dots). g. As in f, but for fixed τ_s and varying g (along the grey dashed line in panel a).

common to all units (t_0)

$$\phi_i = (t_{peak}^i - t_0)\omega_0 \quad \text{modulo} \quad 2\pi. \quad (7)$$

Correspondingly, the amplitude of each unit was defined as the peak-to-peak amplitude $|\delta x_i|$. The phases of different units appear to be uniformly distributed over $[0, 2\pi]$ (Fig. 4 d). In consequence the average population activity is constant in time, so that oscillations are apparent only on the level of individual units, but not on the population-average level.

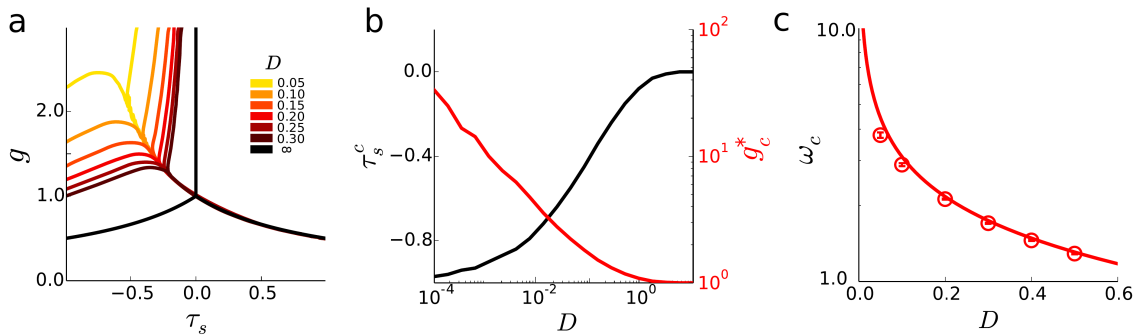


FIG. 3. Effects of interaction delay on network dynamics. a. Bifurcation diagram for different values of interaction delay D . b. Values of τ_s^c and corresponding coupling g_c^* as function of delay. c. Bifurcation frequency as a function of the normalized delay ($\tau_s = -0.7$, g adjusted). Full line: theoretical prediction; red dots: simulation results ($N = 500$, $n = 5$, mean \pm sem).

This was further confirmed by looking at the autocorrelation function of individual units, averaged over the network

$$C(\tau) = \frac{1}{N} \sum_{i=1}^N \int_{-\infty}^{+\infty} x_i(t)x_i(t-\tau)dt \quad (8)$$

which showed clear oscillations. In contrast, the auto-correlation of network-averaged activity

$$K(\tau) = \frac{1}{N^2} \int_{-\infty}^{+\infty} \sum_{i=1}^N x_i(t) \sum_{i=1}^N x_i(t-\tau)dt \quad (9)$$

was flat.

The structure of the oscillatory activity can be understood from the linear analysis close to the instability. In the limit when a single eigenvalue crosses the instability (Fig. 4a-f), the oscillations are predicted to occur along a single mode:

$$x_i(t) \sim e^{i\omega_c t} R_i^{(0)} + \text{c.c.} \quad (10)$$

where $\{R_i^{(0)}\}_{i=1\dots N}$ is the right eigenvector of J corresponding to the unstable eigenvalue $\lambda_0 = i\omega_c$. Within this limit, all the units share the same oscillation frequency, and the distribution of amplitudes and phases of the different units is determined by the amplitudes and phases of the eigenvector $\{R_i^{(0)} = A_i e^{i\Phi_i}\}_{i=1\dots N}$. A comparison with the simulations shows that close to the instability, the phases and amplitudes of individual units are indeed perfectly predicted by the phases and amplitudes of the unstable eigenvector (Fig. 4e,f). The

dynamics are therefore effectively one-dimensional, and the random amplitudes and phases of the oscillation are a direct consequence of the random distribution of the elements of the corresponding eigenvector (A_i and Φ_i respectively).

As the coupling is further increased above g_c , an increasing number of modes become unstable and the dynamics become more complex. The envelope of the oscillations starts to fluctuate (Fig. 5b), and the envelope of the auto-correlation function of individual units displays a slow decay (Fig. 5c). This damping of oscillations may reveal underlying chaotic dynamics, an issue we have not explored further. The individual phases and amplitudes are not anymore accurately predicted by the first eigenvector (Fig. 5e,f), yet the phases of individual units remain uniformly distributed on $[0, 2\pi]$ (Fig. 5d), so that the summed population activity is constant. The network therefore remains in a heterogeneous oscillatory state, in which individual units strongly oscillate, but this oscillation is not apparent on the population-average level.

To further quantify the dimensionality of the dynamics, we have computed projections of the activity on the left eigenvectors of the coupling matrix, defined as

$$\frac{1}{T} \sum_{t=1}^T \langle L^i | x_t \rangle / \|x_t\|. \quad (11)$$

with T being the length of the time-window used for all computations ($T = 10^7$). As the coupling is increased, the number of non-zero projections increases. This can be seen both when looking at all the sorted modes with a fixed coupling (Fig. 6a) or varying the coupling for a fixed eigenmode (Fig. 6b). The oscillatory state explores more and more dimensions as the coupling is increased above the instability.

V. DISCUSSION

In summary, we have described a heterogeneous oscillatory state in randomly coupled networks units with delayed and partially anti-symmetric interactions. This oscillatory state is governed by a novel type of bifurcation, in which a continuum of eigenvalues crosses the instability line at a non-zero frequency. In this state, individual units oscillate with random phases, so that the summed population activity remains constant in time.

From this perspective, the heterogeneous oscillatory state bears some similarity with the splay-state, an asynchronous regime in networks of interacting oscillators [13, 14]. One

important difference is that in the classical splay state the individual units oscillate even in absence of coupling. In contrast, in the network considered here, the individual units are not intrinsic oscillators. In absence of coupling, their activity is constant in time, and the oscillations appear only when the coupling increases beyond a critical value. Note also that while both the splay state and the heterogeneous oscillatory state are “asynchronous” in the sense that the macroscopic activity displays no oscillations, they are distinct from other types of asynchronous states [7, 15, 16] in which the individual units do not oscillate.

The instability described here is also related to the oscillatory Turing instability described in the context of random ecological networks [17]. That bifurcation is also generated by a continuous part of the eigenspectrum of the stability matrix, and leads to heterogeneous oscillations in which different nodes in the network oscillate out of phase. The underlying mechanism is however different as in Ref. [17] the interactions between nodes are symmetric and not delayed.

Following previous works, we considered here a simplified network with a Gaussian connectivity matrix, and a transfer function symmetric around zero. Such a model does not implement basic biophysical constraints such as segregation between excitatory and inhibitory neurons, or the requirement that neural activity is positive. The influence of such constraints on the zero-frequency instability to rate chaos have been investigated recently in a series of works [7, 8, 18, 19]. These studies focused on the asymmetric case. Determining how the heterogeneous oscillatory state described here occurs in more realistic networks will require combining excitation-inhibition segregation with symmetry (or asymmetry) in the connections. This represents an additional challenge, as both ingredients influence the spectrum of the interaction matrix. Note that reciprocal connections between excitatory and inhibitory cells may represent a natural source of anti-symmetric connectivity. Such connections have been in particular reported in the olfactory bulb, and linked to the gamma oscillations occurring there [20]. It would be interesting to investigate further whether these oscillations are related to the phenomenon described here.

Oscillatory activity is widespread in biological networks, and in particular in the brain [21]. Possible origins of these oscillations have mainly been conceptualized in terms of bifurcations in low-dimensional dynamical systems. Together with other recent results [22], this study suggest that high-dimensional, disordered networks can lead to novel oscillatory mechanisms that should be taken into account when interpreting biological data.

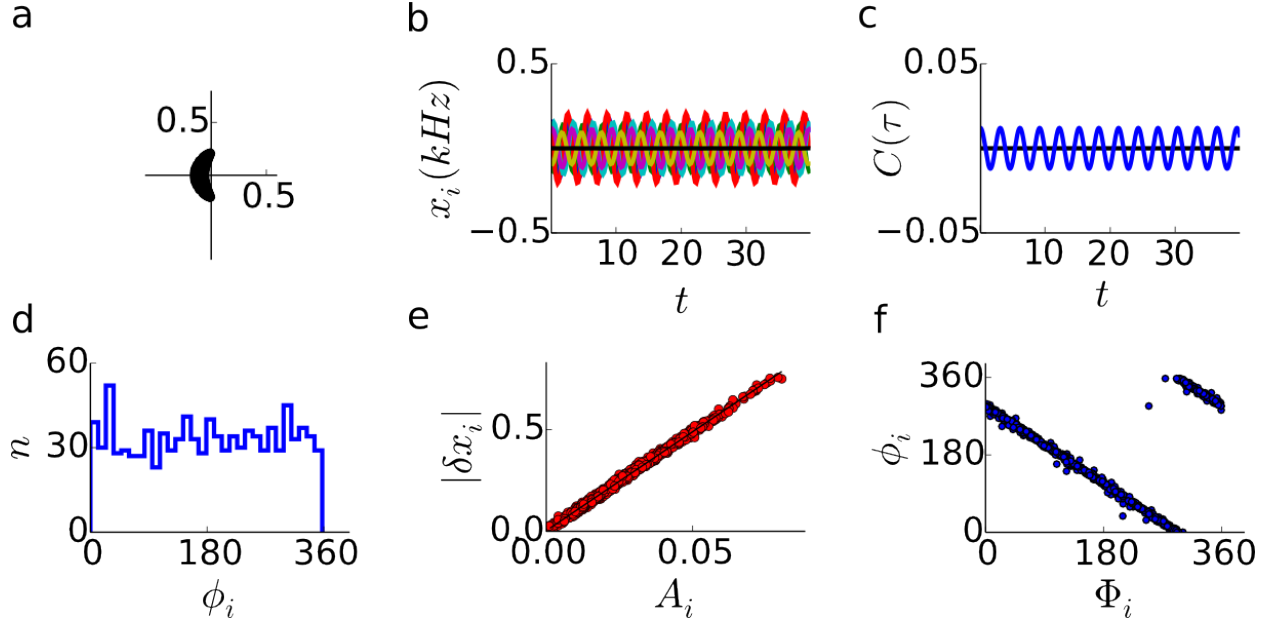


FIG. 4. Heterogeneous oscillations just above the instability ($g = 1.4$). Example simulation with only one λ with a positive real part ($g = 1.4$). The connection matrix was found so that only one eigenvalue was unstable. The simulations were performed using $\tau_s = -0.7$ and $D = 0.2$ ($N=1000$). a. Distribution of the computed λ . b. Firing rate of 10 neurons superimposed. c. Mean auto-correlogram of all neurons $C(\tau)$ (blue trace) and auto-correlogram of the mean population activity $K(\tau)$ (black). d. Histograms of the phases of the firing rates of all neurons. e. Correlation between the amplitudes of the firing rates and the module of each component of the principal eigenvector. f. Correlation between the phases of the firing rates and the phase of each component of the principal eigenvector.

ACKNOWLEDGEMENT

We are grateful to Vincent Hakim for discussions. This work was funded by the Programme Emergences of City of Paris, and the program “Investissements d’Avenir” launched by the French Government and implemented by the ANR, with the references ANR-10-LABX-0087 IEC and ANR-11-IDEX-0001-02 PSL* Research University.

[1] S. H. Strogatz, Westview press. (2014)

[2] H. Sompolinsky, A. Crisanti, and H. J. Sommers, Phys. Rev. Lett. 61, 259 (1988)

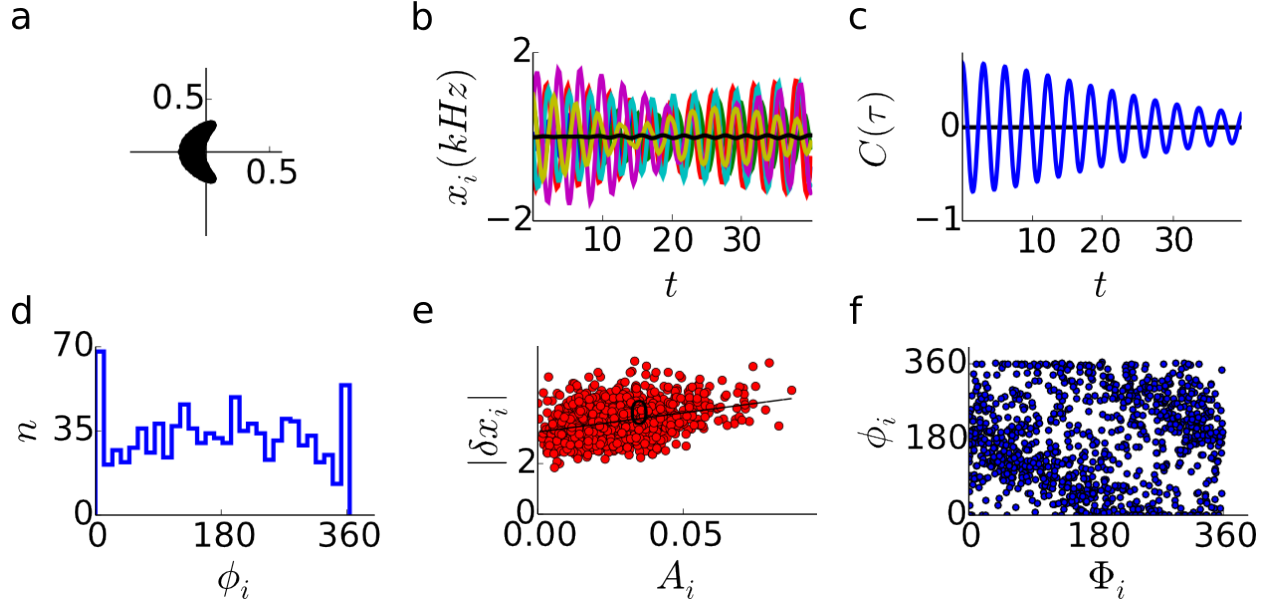


FIG. 5. Same as Fig. 4, but further above the instability ($g = 2.0$), where several eigenvalues have crossed the instability line.

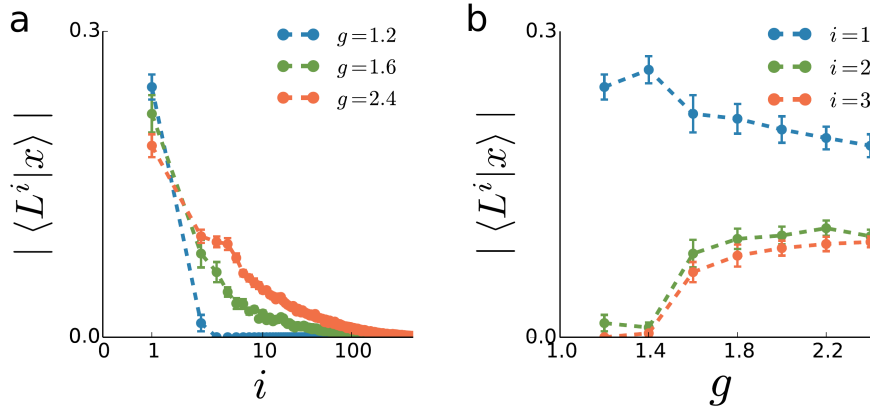


FIG. 6. Dimensionality of the dynamics above the oscillatory instability. a. Projection of network activity x on the left eigenvector associated to the different eigenvalues, ordered by decreasing real part, for increasing coupling g (conjugate eigenvectors are not shown). b. Projection of x on the left eigenvector associated to the first, second or third eigenvalues as a function of g . Parameter values: $\tau_s = -0.7$ and $D = 0.2$, $N=1000$, $n=30$, mean \pm sem.

[3] D. Sussillo, L. F. Abbott, Neuron 63, 544557 (2009)

[4] R. Laje, D. V. Buonomano, Nature Neuroscience 16, 925933 (2013)

[5] G. Wainrib, J. Touboul, Phys. Rev. Lett. 110, 118101, (2013)

- [6] T. Toyozumi, L. F. Abbott, *Phys. Rev. E* 84, 051908 (2011)
- [7] S. Ostojic, *Nature Neuroscience* 17, 594600 (2014)
- [8] J. Kadmon, H. Sompolinsky, *Phys. Rev. X* 5, 04103 (2015)
- [9] P. Dayan, L. Abbott, MIT Press, Cambridge, Mass. (2001)
- [10] H. Sommers, A. Crisanti, H. Sompolinsky, and Y. Stein, *Phys. Rev. Lett.* 61, 259 (1988)
- [11] J. Bélair, *Journal of Dynamics and Differential Equations* 5, 607 (1993)
- [12] C. Marcus and R. Westervelt, *Phys. Rev. A* 39, 347 (1989)
- [13] L. F. Abbott, C. van Vreeswijk, *Phys Rev E* 48(2):1483-1490. (1993)
- [14] L. Tattini, S. Olmi, A. Torcini, *Chaos* 22, 023133 (2012)
- [15] A. Renart, J. de la Rocha, P. Bartho, L. Hollender, N. Parga, A. Reyes, A., & K. D. Harris, *Science*, 327(5965): 587590. (2010)
- [16] N. Brunel, *N. J Comput Neurosci* 8: 183. (2000)
- [17] S. Hata, H. Nakao, A. S. Mikhailov, *Scientific Reports* 4, 3585 (2014)
- [18] O. Harish, D. Hansel, *PLoS Comput Biol* 11(7): e1004266 (2015)
- [19] F. Mastroguiseppe and S. Ostojic, arXiv, submitted. (2016)
- [20] Z. Li, J. Hopfield, *Phys. Rev. Lett.* 97, 188104 (2006)
- [21] G. Buzsáki, Oxford University Press. (2006)
- [22] L. C. G. Del Molino, K. Pakdaman, J. Touboul, G. Wainrib, *Physical Review E* 88 (4), 042824L (2013)